Editors' Suggestion

Activation and electron spin resonance of near-surface implanted bismuth donors in silicon

D. Holmes,[1,*] W. I. L. Lawrie,[1] B. C. Johnson,[1] A. Asadpoordarvish,[2] J. C. McCallum,[1] D. R. McCamey,[2] and D. N. Jamieson[1]

[1]*Centre for Quantum Computing and Communication Technology, School of Physics, The University of Melbourne, Melbourne, Victoria 3010, Australia*

[2]*ARC Centre of Excellence in Exciton Science, School of Physics, The University of New South Wales, Sydney, New South Wales 2052, Australia*

(Received 29 May 2019; published 29 August 2019)

The bismuth (Bi) substitutional donor in silicon (Si) is an attractive qubit candidate for quantum computing proposals due to its large Hilbert space, clock transitions, and potential to couple to superconducting flux qubits. Single-qubit control, coupling, and readout by surface nanocircuitry requires a Bi depth of ∼20 nm in Si. This can be achieved using ion implantation of ∼25 keV Bi. This work explores the activation properties of Bi implanted at 26 keV with fluences of 1×10^{14} and 6×10^{12} cm^{-2} into both crystalline and preamorphized Si. The Bi electrical activation yield was measured over a broad range of annealing conditions using resistivity and Hall effect measurements, enabling optimal annealing strategies to be proposed for the different implant parameters. For the high and low fluences, the maximum Bi activation yields achieved were 64% and 46%, respectively. Above a critical thermal budget, a substantial fraction of Bi forms electrically inactive complexes in the high fluence sample only. The substitutional fraction and diffusion of high fluence Bi was quantified, with diffusion coefficients $D_0 = 4.0 \pm 0.5$ and 7.5 ± 0.5 cm^2 s^{-1} found for implantation into crystalline and preamorphized Si, respectively, using Rutherford backscattering spectrometry. To demonstrate the successful activation and quantum control of near-surface implanted Bi, the full hyperfine spectrum of these donors is obtained using continuous-wave electron spin resonance at 25 K, supporting the suitability for Bi donor qubits.

DOI: 10.1103/PhysRevMaterials.3.083403

I. INTRODUCTION

Quantum computing proposals involving group V donor qubits in silicon (Si) have attracted considerable interest in recent years. The "semiconductor vacuum" of isotopically pure ^{28}Si offers long electron and nuclear spin coherence times [1] desirable for high-fidelity qubit operation. Donor qubits have been realized for phosphorus in Si using surface electrodes for readout and control of the electron and nuclear spin states [2–4], leading to various quantum computing architectures [5–7] to be proposed. Of interest is the bismuth (Bi) donor, which offers technological advantages including its potential for use as a quantum memory due to the large nuclear spin ($I = 9/2$) providing a 20-dimensional Hilbert space [8]. Bi donors exhibit clock transitions [9] where the transition frequency to first-order is insensitive to magnetic-field variations offering increased coherence times. The large zero-field splitting of 7.4 GHz also could allow Bi spin qubits to be coupled to superconducting flux qubits [10–12].

Readout and control of spin qubits by surface nanocircuitry require a sparse density of donors commonly placed ∼20 nm below the Si-oxide interface [7], as illustrated in Fig. 1. A promising solution for fabricating such donor devices in Si is low-energy, low-fluence ion implantation. With this method, Bi offers increased qubit placement precision over other group V donors due to its reduced longitudinal straggle of 4.0 nm compared to 9.2 nm for phosphorus when implanted to a mean projected range of 20 nm in Si, based on Monte Carlo simulations using the software SRIM [13]. Deterministic ion implantation technology [14–17] provides a possible pathway for creating a scalable array of single donors required for quantum computing architectures.

The high atomic mass of Bi, however, results in a dense damage profile upon implantation. Bi also has a low equilibrium solid solubility limit of 8×10^{17} cm^{-3} at 1320 °C [18], which poses a challenge in obtaining a workable active Bi concentration in Si. Achieving operational Bi donor qubits requires an annealing scheme that results in a high electrical activation yield (i.e., a high fraction of donors that have one electron available to donate to the conduction band), a high fraction of substitutional donors in the Si lattice, and a measurable electron spin resonance (ESR) spectrum. Diffusion during annealing must be limited as this causes an increase in donor placement uncertainty and may decrease the donor density in the active device area. Channeling of implanted ions down crystal axes can also increase donor placement uncertainty. This can be avoided by amorphizing the Si with a sufficiently high fluence implant of ^{28}Si ions, selected using a mass spectrometer, before the implantation of Bi, here termed "preamorphization." The ^{28}Si isotope was chosen due to its high abundance and zero nuclear spin.

To date, annealing studies on the electrical activation [19–24], substitutional fraction [19,25,26], and diffusion [27] of Bi implanted Si have not considered the effect of the

*Author to whom all correspondence should be addressed: dholmes1@student.unimelb.edu.au

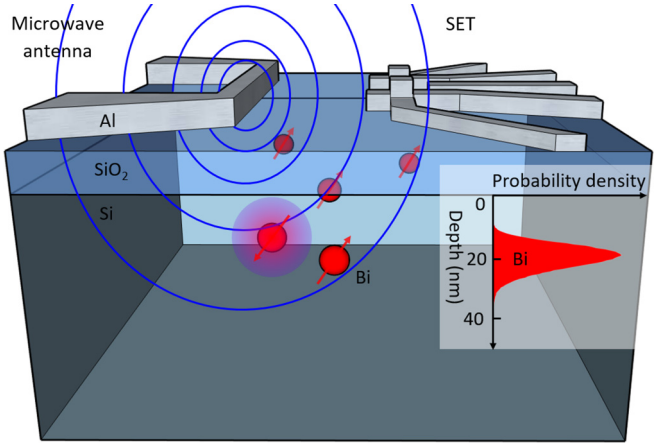

FIG. 1. An example of a proposed donor qubit device (not to scale) with implanted Bi donors (red). Donors are located ∼20 nm below the Si-oxide interface enabling spin manipulation by an on-chip microwave antenna and readout by coupling to a single-electron transistor (SET). The inset shows the depth profile of implanted 26 keV Bi donors simulated using SRIM. Control and readout of a single Bi donor could be achieved by tuning the potential of surface gates [1].

preamorphization of Si. Previously, the 10 ESR transitions corresponding to the Bi nuclear spin, $I = 9/2$, have been obtained on electrically activated Bi donors in natural Si [12,28] and ^{28}Si [29], with spin-dependent recombination-based magnetic resonance spectroscopy [30] and bound exciton photoluminescence [31]. Yet these experiments were performed on Bi donors implanted to depths between 35 and 150 nm [29,30] or incorporated into the bulk of Si using the pedestal technique [32] during float zone growth [12,28,31].

This work considers the effect of a preamorphization implant (PAI) and annealing on the activation of Bi donors implanted to a depth of 20 nm at fluences above and below the Si amorphization threshold. Optimal activation strategies are proposed by determining the dependence of carrier concentration, calculated using resistivity and Hall effect measurements, and substitutional fraction and diffusion, measured using Rutherford backscattering spectrometry (RBS), on implant and anneal parameters. The full hyperfine spectrum of implanted Bi donors, solely residing near the Si surface, was obtained using ESR to confirm successful activation.

II. EXPERIMENT

Highly intrinsic (4–10 kΩ cm), float zone natural Si (UHPS Topsil) was implanted at room temperature with 26 keV Bi with a tilt angle of 7° to suppress channeling. A SRIM (v2013) simulation with Bi implanted into Si at this energy and angle of incidence gave a mean projected range of 20 nm. The preamorphization parameters and Bi fluences investigated in this work are specified in Table I. The fluences of 6×10^{12} and 1×10^{14} cm^{-2} were chosen to straddle the Si amorphization threshold. The maximum concentration and corresponding minimum Bi spacing at the peak of the depth profile for these fluences were calculated using the SRIM simulation and shown in Table I. After implantation and a piranha (4:1 98% H_2SO_4 : 30% H_2O_2, 90 °C) and RCA-2 (5:1:1 H_2O : 30% H_2O_2 : 36% HCl, 70 °C) clean, samples A–D were given a rapid thermal anneal (RTA) in Ar atmosphere at a range of temperatures, 600–1000 °C, and durations, 5–300 s.

TABLE I. Implant parameters investigated for samples A–D.

Implantation step	Sample			
	A	B	C	D
^{28}Si PAI (keV, cm^{-2})	None	None	20, 1×10^{15}	20, 1×10^{15}
Bi implant (keV, cm^{-2})	26, 6×10^{12}	26, 1×10^{14}	26, 6×10^{12}	26, 1.0×10^{14}
Max. Bi conc. (cm^{-3})	6.3×10^{18}	1.0×10^{20}	6.3×10^{18}	1.0×10^{20}
Min. Bi spacing (nm)	5.4	2.1	5.4	2.1

Samples A–D then underwent a HF etch to remove the native oxide, and 200 nm of Al was evaporated onto the corners exposed by a shadow mask. A forming gas (Ar:H) anneal at 400 °C for 30 min was used to ensure good Ohmic contacts. Resistivity and Hall effect measurements were taken at room temperature using Van der Pauw devices with a magnetic-field sweep between −0.7 and 0.7 T at currents of 5 μA. The Bi electrical activation yield was calculated by dividing the measured effective carrier sheet density, determined from Hall measurements, by the total implanted fluence. The measured carrier sheet density of the intrinsic substrate was negligible and so the Hall measurements can be assumed to be probing solely the electrons provided by the Bi donors.

RBS measurements were performed on a 5U Pelletron accelerator with 1 MeV ^{4}He$^+$ ions using detectors positioned at 110° and 170° scattering angles. For the high fluence Bi samples B and D, the substitutional fraction, f, of Bi donors on lattice sites to the total number of donors present was measured using [33]

$$f = \frac{1 - \chi_I}{1 - \chi_R}, \tag{1}$$

where χ_I and χ_R are the proportions of the integrated area of the Bi peak and the Si edge height in the RBS spectra for the channeled orientation, with the ^{4}He$^+$ beam aligned along a ⟨100⟩ crystal direction in this work, to the random orientation, where the beam is not aligned with any low-index crystal directions or planes, respectively,

$$\chi_I = \frac{A(\mathrm{Bi,C})}{A(\mathrm{Bi},R)}, \tag{2}$$

$$\chi_R = \frac{H(\mathrm{Si,C})}{H(\mathrm{Si},R)}. \tag{3}$$

These parameters are shown in the channeled and random RBS spectra in Fig. 2(b). Bi depth profiles were fitted with Gaussian curves, and the full width at half-maximum (FWHM) was extracted, enabling a quantitative measure of Bi diffusion coefficients.

To independently confirm the presence of near-surface implanted and successfully annealed Bi in Si, continuous-wave electron spin resonance (cw-ESR) measurements were

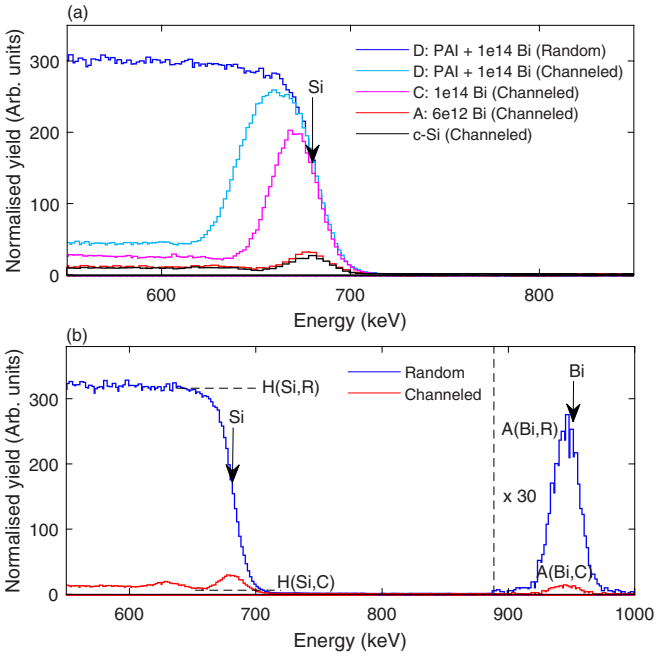

FIG. 2. 1 MeV He^+ RBS spectra collected at a scattering angle of 110°. (a) The damage to the Si crystal caused by the various implants in Table I before annealing can be seen in the Si edge height in the channeled orientation. (The legend is in order of decreasing Si edge height.) (b) Sample D annealed at 700 °C for 5 min. With the sample aligned in the channeled orientation, the Si surface peak and lower energy peak corresponding to channeling oscillation [36] are visible. The reduced area of the Bi peak for the channeled sample orientation is due to the high substitutional fraction.

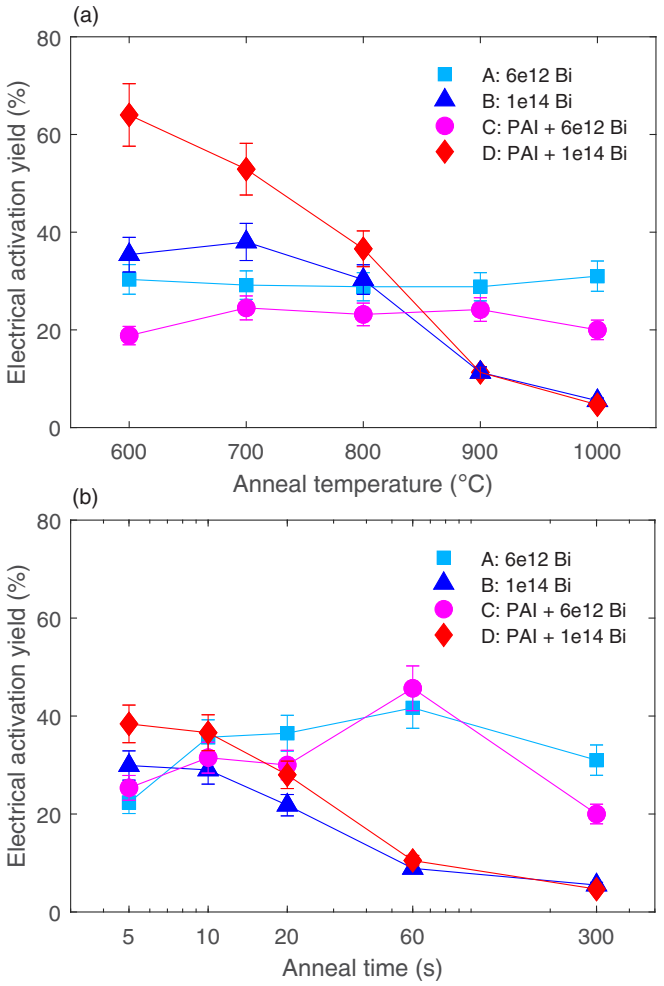

FIG. 3. Electrical activation yield of Bi implanted Si given (a) a 5 min RTA at various temperatures and (b) a 1000 °C RTA for various times. Errors are dominated by the uncertainty in the implant fluence.

carried out on a 6×10^{12} cm^{-2} Bi implanted sample using a Bruker Elexsys II ESR Spectrometer in an X-Band cavity at 9.7209 GHz. The magnetic field was swept between 0 and 600 mT at 25 K. The microwave power was set to 0.4743 mW and the magnetic field was modulated at a frequency of 100 kHz and an amplitude of 0.1 mT.

III. RESULTS AND DISCUSSION

Bi implantation fluences in this work were chosen to straddle the Si amorphization threshold, where a continuous amorphous layer is formed at $\gtrsim 1 \times 10^{14}$ cm^{-2} for keV Bi ions [34]. This was confirmed by Raman spectroscopy (not shown) and from the height of the Si edge in the RBS spectra for samples in the channeled orientation, shown in Fig. 2(a). A Bi fluence of 6×10^{12} cm^{-2} was shown not to result in a continuous amorphous layer, as the channeled RBS spectrum from sample A closely matches that produced by a crystalline Si (*c*-Si) sample without implantation. Comparisons with simulations using the RBS software RUMP [35] suggest that a continuous amorphous Si layer is present after implanting 1×10^{14} Bi cm^{-2} (sample C). The RBS spectrum for sample D with a PAI has a wider Si edge that is consistent with a thicker amorphous layer. The height of the channeled edge does not reach that of the random edge due to the thickness of the amorphous layer and a detector energy FWHM of 25 keV, as calculated by matching the shape of the Si edge with RUMP simulations.

Sections of samples A–D underwent an RTA at temperatures between 600 and 1000 °C for 5 min. Bi electrical activation yield data are shown in Fig. 3(a). A significant decrease in Bi activation is observed at temperatures above 800 °C for high fluence samples B and D. This is in agreement with previous studies of Bi implanted at fluences above the Si amorphization threshold, where a maximum electrical activation yield, up to ~90% [19], is achieved for temperatures around 600–700 °C for a few minutes [19–21,23]. The high fluence implant exceeds the Si amorphization threshold and so crystallization proceeds via solid phase epitaxy (SPE) [37] in which Bi donors are incorporated onto substitutional sites (a metastable state), often above the solid solubility limit. The decrease in Bi activation observed above 800 °C may be a result of an increased thermal budget allowing the Bi to move off lattice sites into interstitial sites (an equilibrium configuration), resulting in deactivation. Bi diffusion at these high temperatures was also observed using RBS, as described below, which supports this theory. A PAI produces a thicker, and likely more homogeneous amorphous layer, than 1×10^{14} Bi cm^{-2} alone, which therefore increases Bi activation for low-temperature anneals by aiding the SPE regrowth

mechanism. For implant fluences below the Si amorphization threshold, higher-temperature anneals of around 900 °C have been shown to maximize Bi activation [22,24,29]. However, for the implant parameters considered in this work, no significant dependence on anneal temperature is observed. The PAI in this case results in a slightly lower activation yield of 22% on average, whereas without the PAI, the yield is closer to 30%.

Sections of samples A–D underwent an RTA at 1000 °C for durations between 5 and 300 s. The Bi electrical activation yield data for these samples are shown in Fig. 3(b). For high fluence samples B and D, a shorter anneal time of 5 s maximizes Bi activation for high-temperature annealing but does not come close to the higher level of activation achieved at 600 °C. For low fluence samples A and C, Bi activation increases with anneal time from 5 to 60 s but then drops when further increased to 300 s. The decrease in electrical activation for the high fluence case occurs at lower thermal budgets than the low fluence case. This could be explained due to the higher fraction of Bi above the equilibrium solubility limit, which can be deactivated in the high fluence case.

Optimal Bi electrical activation yields in the low and high fluence regimes were found to be 46% and 64%, corresponding to active concentrations of around 2.0×10^{18} and 6.6×10^{19} cm^{-3} at the implant profile peak estimated using SRIM and taking into account diffusion as measured by RBS, respectively. These active concentrations are well above the equilibrium solid solubility limit of 8×10^{17} cm^{-3} [18]. This agrees with previous studies of ion-implanted Si, where SPE can produce a metastable substitutional solid solution, where the Bi solubility limit can be as high as 9×10^{19} cm^{-2} [38]

For high fluence samples B and D, the Bi substitutional fraction as a function of anneal temperature and time is shown on the left axes in Fig. 4. In general, almost all of the implanted Bi is substitutional in the Si lattice after 5 min anneals between 600 and 800 °C and for 1000 °C anneals between 5 and 20 s. The substitutional fraction drops above 800 °C for 5 min anneals and above 20 s for 1000 °C anneals, in agreement with previous studies [19,21,23]. With increasing applied thermal budget, more of the Bi donors are displaced from metastable lattice site locations and become stable interstitial defects. This aids the understanding of the observed trends in electrical activation yield for the high fluence Bi samples.

The maximum electrical activation yields measured are significantly lower than the near 100% substitutional fraction of high fluence samples B and D as measured by RBS. This could be due to a number of possible causes, including an abundance of interface traps, oxide charge due to low-quality native oxides, or strain-induced electric fields due to lattice mismatch between Si and its oxide and due to the large covalent radius mismatch between Bi and Si. Since the present RBS measurements were performed with channeling along only the ⟨100⟩ axis, the actual substitutional fraction could be lower than measured if Bi is displaced from lattice sites but hidden from the He^+ ion beam. This was found in a previous study, with similar implant fluence and annealing conditions, in which RBS measurements were taken using an angular scan across the ⟨100⟩ axis to determine that a fraction of the Bi atoms that were apparently substitutional when measured in the ⟨100⟩ direction are in fact slightly displaced from crystal rows [19].

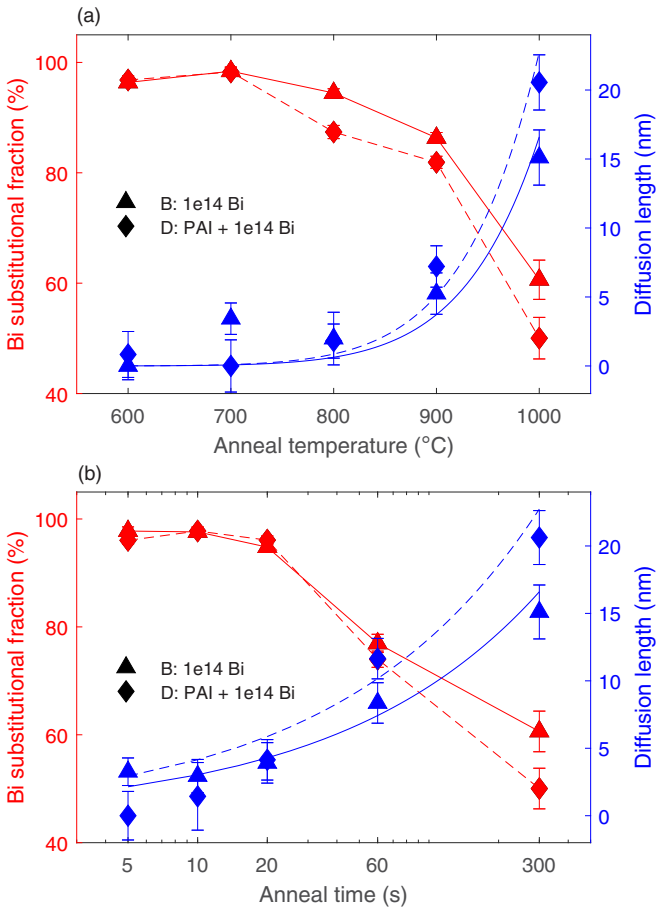

FIG. 4. (a) The substitutional fraction of Bi measured using RBS at a scattering angle of 170° (red) and the diffusion length of Bi measured from the FWHM of the Bi peak in RBS spectra collected at a scattering angle of 110° (blue) as a function of anneal temperature for a 5 min RTA. (b) The same as a function of anneal time for a 1000 °C RTA. The diffusion length data were fit with Eqs. (7) and (5) with a fixed activation energy $E_A = 3.85$ eV [39], resulting in diffusion coefficients of $D_0 = 4.0 \pm 0.5$ and 7.5 ± 0.5 cm^2 s^{-1} in samples without and with preamorphization, respectively. Error bars are estimated from the RBS spectra (red) and the standard deviation of Gaussian fitting to the depth profiles (blue).

Bi depth profiles in randomly oriented RBS spectra were fit with Gaussian curves to extract the FWHM to determine the extent of diffusion during annealing. Broadening of a Gaussian dopant profile [40] can be described by Fickian diffusion where the donor concentration, n, at a depth below the surface, x, is given by

$$n(x) \propto \exp(-(x - R_p)^2/2(\sigma^2 + 2Dt))\ \text{cm}^{-3} \qquad (4)$$

with a projected range, R_p, a standard deviation of the Gaussian profile before annealing, σ, and anneal time, t. The dopant diffusivity, D, at a temperature T is given by

$$D = D_0 \exp(-E_A/k_B T)\ \text{cm}^2/\text{s} \qquad (5)$$

with a diffusion coefficient, D_0, and an activation energy, E_A [39]. The measured FWHM of the Bi peak can be

expressed as

$$\mathrm{FWHM} = 2.355\sqrt{\sigma^2 + 2Dt + \sigma_E^2}, \tag{6}$$

where the detector energy resolution was modeled as a Gaussian with standard deviation σ_E, which convolves with the Gaussian Bi doping profile. This was used to calculate the diffusion length:

$$l = 2\sqrt{Dt}, \tag{7}$$

which is plotted as a function of anneal temperature and time on the right axes in Fig. 4. Bi diffusion in Si only becomes significant to within the precision of our measurement for anneal temperatures at and above 900 °C for 5 min and for anneal times at and above 60 s for 1000 °C. If the diffusion length is comparable to the mean donor spacing, Bi clustering into undesirable electrically inactive complexes can occur [41]. Since high fluence samples B and D have a smaller mean donor spacing, this can also explain why their Bi activation is significantly decreased at lower thermal budgets compared to low fluence samples A and C. Fickian diffusion curves, described by Eqs. (7) and (5), with an activation energy, E_A, taken to be 3.85 eV [39] were fitted to the data to give diffusion coefficients $D_0 = 4.0 \pm 0.5$ and 7.5 ± 0.5 cm^2 s^{-1} without and with a PAI, respectively. These values are higher than that found for Bi diffusion into crystalline Si from an epitaxially deposited layer of $D_0 = 1.08$ cm^2 s^{-1} [39]. Bi diffusion is vacancy-mediated [42], therefore the Si lattice damage created during ion implantation could enhance diffusion.

The presence of active implanted Bi donors in Si was confirmed using ESR. At X-band, a large magnetic-field range of 0–600 mT is required to collect the complete Bi hyperfine spectrum due to the large nuclear spin ($I = 9/2$) and hyperfine interaction ($A = 1475.4$ MHz) of Bi [44]. The simulated Bi hyperfine energy levels [43] and the cw-ESR data are shown in Fig. 5. Samples are required to be nonmetallic for ESR, therefore a low fluence Bi implant of 6×10^{12} cm^{-2}, with a maximum Bi concentration below the metal-insulator transition ($N_C = 1.8 \times 10^{19}$ cm^{-3}) [45], was chosen. This sample did not have a PAI, and donors were activated with an RTA at 1000 °C for 5 s. A sample area of 0.65 cm^2, resulting in a total of 3.9×10^{12} implanted Bi donors, was laser cut and stacked to fit inside the sapphire cavity of the ESR machine. Assuming an electrical activation yield of 22.4%, as measured from the Van der Pauw devices, this corresponds to a total of 8.7×10^{11} active Bi spins, which produced a measurable signal above the experimental sensitivity limit. The experimental data were collected in 10 subsets, each spanning 10 mT and centered on the expected magnetic field. Each subset was scanned 1000 times to increase the signal-to-noise ratio. The magnetic field between the 10 peaks was not scanned to reduce the data collection time. The background signal due to resonances and defects in the sapphire cavity was fitted and subtracted from the data. The strongest ESR transition signal was found in the second harmonic and is shown here. This can be explained by the saturation of the second-harmonic ESR signal with increasing microwave power being much less than that of the first harmonic [46]. The inset of Fig. 5(b) shows the shape of the second-harmonic ESR signal for the $m_s = +9/2$ transition from which the ESR peak-to-peak linewidth can be extracted

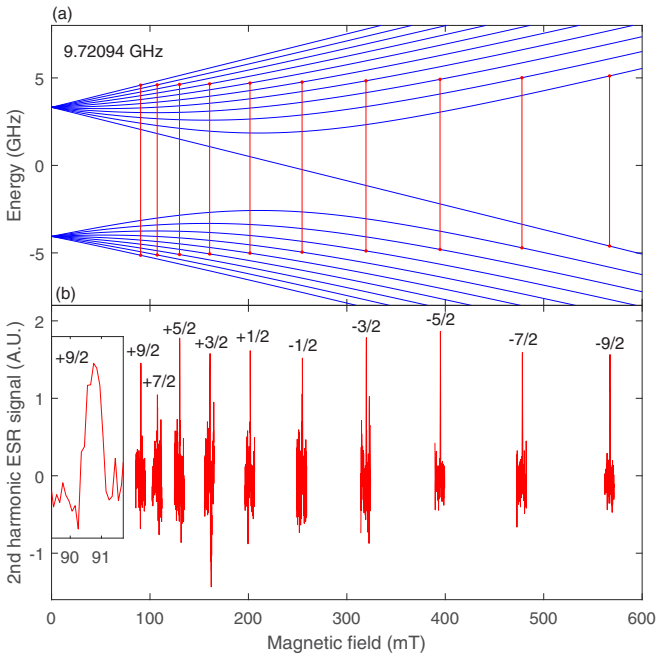

FIG. 5. (a) Simulated energy levels of Bi in Si as a function of magnetic field [43]. The red lines show the magnetic field at which microwaves with frequency 9.7209 GHz are on resonance with an ESR transition. (b) The full hyperfine spectrum of near-surface implanted Bi in Si measured using cw-ESR at $T = 25$ K with a microwave frequency of 9.7209 GHz at 0.4743 mW. The 10 ESR peaks are labeled with their projected nuclear spin, m_s. The inset shows an expanded view of the $m_s = +9/2$ transition.

to be $l_{\mathrm{pp}} = 7.5 \pm 0.5$ G. This is larger than the linewidth of ~4 G measured for Bi incorporated in the bulk of natural Si [12], which could be explained due to the close proximity of the native oxide interface increasing the variation in the local magnetic environment of the Bi. As shown, each of the 10 measured ESR peaks occurs at the expected magnetic field for the given microwave frequency and so agrees with the simulation. The full Bi hyperfine spectrum verifies a successful implantation and annealing strategy for near-surface Bi in Si.

IV. CONCLUSION

In conclusion, optimal implant and annealing strategies for near-surface implanted Bi donors at fluences 1×10^{14} and 6×10^{12} cm^{-2} were found to be solid phase epitaxy at 600 °C for 5 min and an RTA at 1000 °C for 60 s, both following preamorphization, resulting in electrical activation yields of 64% and 46%, respectively. The substitutional fraction and diffusion of Bi were measured to aid the explanation of the trends found. The full Bi hyperfine spectrum containing all 10 transitions was obtained for Bi donors implanted to a depth of ≈20 nm below the native oxide interface and subsequently annealed. This confirms the successful annealing of the damaged Si lattice caused by heavy-ion implantation and the electrical activation of a significant fraction of the Bi donors. These results show promise for Bi donor implantation as a method for fabricating near-surface spin qubits that could be coupled to surface control and readout circuitry for integration into a large-scale device that exploits the unique properties of

Bi. With a Bi donor environment of isotopically pure ^{28}Si, the removal of ^{29}Si nuclear spins would decrease the ESR signal linewidths and prolong coherence times, which are desirable attributes for an engineered device.

ACKNOWLEDGMENTS

This research was funded by the Australian Research Council Centre of Excellence for Quantum Computation and Communication Technology (CE170100012) and the Australian Research Council Centre of Excellence in Exciton Science (Grant No. CE170100026). We acknowledge the AFAiiR node of the NCRIS Heavy Ion Capability for access to ion-implantation facilities and the support of the International Atomic Energy Agency through the Cooperative Research Program No. F11020 "Ion beam induced spatio-temporal structural evolution of materials: Accelerators for a new technology era."

[1] J. T. Muhonen, J. P. Dehollain, A. Laucht, F. E. Hudson, R. Kalra, T. Sekiguchi, K. M. Itoh, D. N. Jamieson, J. C. McCallum, A. S. Dzurak *et al.*, Nat. Nanotechnol. **9**, 986 (2014).

[2] J. J. Pla, K. Y. Tan, J. P. Dehollain, W. H. Lim, J. J. L. Morton, D. N. Jamieson, A. S. Dzurak, and A. Morello, Nature (London) **489**, 541 (2012).

[3] J. J. Pla, K. Y. Tan, J. P. Dehollain, W. H. Lim, J. J. L. Morton, F. A. Zwanenburg, D. N. Jamieson, A. S. Dzurak, and A. Morello, Nature (London) **496**, 334 (2013).

[4] A. Laucht, J. T. Muhonen, F. A. Mohiyaddin, R. Kalra, J. P. Dehollain, S. Freer, F. E. Hudson, M. Veldhorst, R. Rahman, G. Klimeck *et al.*, Sci. Adv. **1**, e1500022 (2015).

[5] C. D. Hill, E. Peretz, S. J. Hile, M. G. House, M. Fuechsle, S. Rogge, M. Y. Simmons, and L. C. L. Hollenberg, Sci. Adv. **1**, e1500707 (2015).

[6] G. Pica, B. W. Lovett, R. N. Bhatt, T. Schenkel, and S. A. Lyon, Phys. Rev. B **93**, 035306 (2016).

[7] G. Tosi, F. A. Mohiyaddin, V. Schmitt, S. Tenberg, R. Rahman, G. Klimeck, and A. Morello, Nat. Commun. **8**, 450 (2017).

[8] G. W. Morley, M. Warner, A. M. Stoneham, P. T. Greenland, J. Van Tol, C. W. Kay, and G. Aeppli, Nat. Mater. **9**, 725 (2010).

[9] G. Wolfowicz, A. M. Tyryshkin, R. E. George, H. Riemann, N. V. Abrosimov, P. Becker, H.-J. Pohl, M. L. W. Thewalt, S. A. Lyon, and J. J. L. Morton, Nat. Nanotechnol. **8**, 561 (2013).

[10] I. Chiorescu, Y. Nakamura, C. J. P. M. Harmans, and J. E. Mooij, Science **299**, 1869 (2003).

[11] X. Zhu, S. Saito, A. Kemp, K. Kakuyanagi, S.-i. Karimoto, H. Nakano, W. J. Munro, Y. Tokura, M. S. Everitt, K. Nemoto *et al.*, Nature (London) **478**, 221 (2011).

[12] R. E. George, W. Witzel, H. Riemann, N. V. Abrosimov, N. Nötzel, M. L. W. Thewalt, and J. J. L. Morton, Phys. Rev. Lett. **105**, 067601 (2010).

[13] J. F. Ziegler, M. D. Ziegler, and J. P. Biersack, Nucl. Instrum. Methods Phys. Res., Sect. B **268**, 1818 (2010).

[14] M. B. H. Breese, E. Vittone, G. Vizkelethy, and P. J. Sellin, Nucl. Instrum. Methods Phys. Res., Sect. B **264**, 345 (2007).

[15] B. C. Johnson, G. C. Tettamanzi, A. D. C. Alves, S. Thompson, C. Yang, J. Verduijn, J. A. Mol, R. Wacquez, M. Vinet, M. Sanquer *et al.*, Appl. Phys. Lett. **96**, 264102 (2010).

[16] J. Van Donkelaar, C. Yang, A. D. C. Alves, J. C. McCallum, C. Hougaard, B. C. Johnson, F. E. Hudson, A. S. Dzurak, A. Morello, D. Spemann *et al.*, J. Phys.: Condens. Matter **27**, 154204 (2015).

[17] D. N. Jamieson, W. I. L. Lawrie, S. G. Robson, A. M. Jakob, B. C. Johnson, and J. C. McCallum, Mater. Sci. Semicond. Proc. **62**, 23 (2017).

[18] F. A. Trumbore, Bell Syst. Technol. J. **39**, 205 (1960).

[19] J. P. De Souza and P. F. P. Fichtner, J. Appl. Phys. **74**, 119 (1993).

[20] B. L. Crowder, J. Electrochem. Soc. **118**, 943 (1971).

[21] R. Baron, G. A. Shifrin, O. J. Marsh, and J. W. Mayer, J. Appl. Phys. **40**, 3702 (1969).

[22] T. Peach, K. Homewood, M. Lourenco, M. Hughes, K. Saeedi, N. Stavrias, J. Li, S. Chick, B. Murdin, and S. Clowes, Adv. Quantum Technol. **1**, 1800038 (2018).

[23] S. G. Tavakoli, S. Baek, H. S. Chang, D. W. Moon, and H. Hwang, Appl. Phys. Lett. **86**, 032104 (2005).

[24] A. Yamamoto, K. Miki, H. Tanoue, C. H. Lee, H. Takazawa, and T. Ohta, in *Proceedings ICT2001, 20th International Conference on Thermoelectrics (Cat. No. 01TH8589)* (IEEE, Piscataway, NJ, 2001), pp. 306–309.

[25] S. T. Picraux, W. L. Brown, and W. M. Gibson, Phys. Rev. B **6**, 1382 (1972).

[26] A. G. Wagh, S. Radhakrishnan, S. G. Gaonkar, and M. J. Kansara, Nucl. Instrum. Methods **168**, 191 (1980).

[27] T. Schenkel, C. D. Weis, C. C. Lo, A. Persaud, I. Chakarov, D. H. Schneider, and J. Bokor, in *Proceedings of the XII International Symposium on Electron Beam Ion and Traps*, edited by A. Lapierre, S. Schwarz, and T. M. Baumann, AIP Conf. Proc. No. 1640 (AIP, New York, 2015), pp. 124–128.

[28] M. Belli, M. Fanciulli, and N. V. Abrosimov, Phys. Rev. B **83**, 235204 (2011).

[29] C. D. Weis, C. C. Lo, V. Lang, A. M. Tyryshkin, R. E. George, K. M. Yu, J. Bokor, S. A. Lyon, J. J. L. Morton, and T. Schenkel, Appl. Phys. Lett. **100**, 172104 (2012).

[30] P. A. Mortemousque, T. Sekiguchi, C. Culan, M. P. Vlasenko, R. G. Elliman, L. S. Vlasenko, and K. M. Itoh, Appl. Phys. Lett. **101**, 082409 (2012).

[31] T. Sekiguchi, M. Steger, K. Saeedi, M. L. W. Thewalt, H. Riemann, N. V. Abrosimov, and N. Nötzel, Phys. Rev. Lett. **104**, 137402 (2010).

[32] H. Riemann, N. Abrosimov, and N. Noetzel, ECS Trans. **3**, 53 (2006).

[33] W.-K. Chu, *Backscattering Spectrometry* (Elsevier, Amsterdam, 2012).

[34] M. A. Nastasi and J. W. Mayer, *Ion Implantation and Synthesis of Materials* (Springer, Berlin, 2006), Vol. 80 .

[35] L. R. Doolittle, Nucl. Instrum. Methods Phys. Res., Sect. B **9**, 344 (1985).

[36] L. C. Feldman, J. W. Mayer, and S. T. Picraux, *Materials Analysis by Ion Channeling: Submicron Crystallography* (Academic, New York, 2012).

[37] B. C. Johnson, J. C. McCallum, and M. J. Aziz, *Handbook of Crystal Growth: Thin Films and Epitaxy*, 2nd ed. (Elsevier, Amsterdam, 2015), pp. 317–363.

[38] S. T. Picraux, and W. J. Choyke, *Metastable Materials Formation by Ion Implantation* (North-Holland, New York, 1982).
[39] R. N. Ghoshtagore, Phys. Rev. B **3**, 397 (1971).
[40] J. P. Bandyopadhyay, *Solid State Electronic Devices*, 3rd ed. (Vikas Publishing House, New Delhi, 2017).
[41] S. U. Campisano, E. Rimini, P. Baeri, and G. Foti, Appl. Phys. Lett. **37**, 170 (1980).
[42] Y. Ishikawa, I. Kobayashi, and I. Nakamichi, Jpn. J. Appl. Phys. **29**, L1929 (1990).
[43] S. Stoll and A. Schweiger, J. Magn. Reson. **178**, 42 (2006).
[44] M. H. Mohammady, G. W. Morley, and T. S. Monteiro, Phys. Rev. Lett. **105**, 067602 (2010).
[45] E. Abramof, A. F. da Silva, B. E. Sernelius, J. P. De Souza, and H. Boudinov, J. Mater. Res. **12**, 641 (1997).
[46] P. C. Taylor, Characterization of Amorphous Silicon Thin Films and PV Devices: Phase 1 Annual Technical Report No. NREL/SR-520-27298, National Renewable Energy Lab., Golden, CO, 1999.